Biosensors and Bioelectronics ■ (■■■■) ■■■–■■■

Contents lists available at ScienceDirect

Biosensors and Bioelectronics

journal homepage: www.elsevier.com/locate/bios

A novel layer-by-layer assembled multi-enzyme/CNT biosensor for discriminative detection between organophosphorus and non-organophosphrus pesticides

Yuanyuan Zhang [a,1], Mary A. Arugula [a,1], Melinda Wales [b], James Wild [b], Aleksandr L. Simonian [a,*]

[a] Department of Materials Engineering, Auburn University, Auburn, AL 36832, USA
[b] Department of Biochemistry & Biophysics, Texas A&M, College Station, TX, USA

ARTICLE INFO

Article history:
Received 6 June 2014
Received in revised form
1 August 2014
Accepted 16 August 2014

Keywords:
Multi-enzyme
Layer-by-layer self-assembly
Multi-walled carbon nanotube (MWCNT)
Discriminative detection
Paraoxon
Carbaryl

ABSTRACT

Organophosphate compounds are heavily used in agriculture and military activities, while non-organophosphate pesticides are mostly used in agriculture and home defense. Discriminative detection of such toxic compounds is very challenging and requires sophisticated and bulky instrumentation. Meanwhile, multi-enzyme biosensors may offer an effective solution to the problem and may become a versatile analytical tool for discriminative detection of different neurotoxins. In this study, we report for the first time a novel bi-enzyme biosensing system incorporating electrostatically interacted enzyme-armored MWCNT–OPH and MWCNT–AChE along with a set of cushioning bilayers consisting of MWCNT–polyethyleneimine and MWCNT–DNA on glassy carbon electrode for discriminative detection of organophosphorus (OP) and non-organophosphorus (non-OP) pesticides. LbL interfaces were characterized by surface plasmon resonance and electrochemical impedance spectroscopy, demonstrating stepwise assembly and electron conductivity studies. The detection limit was found to be ~0.5 for OP pesticide paraoxon and 1 μM for non-OP pesticide carbaryl, in a wide linear range. The biosensor performance was also validated using apple samples. Remarkable discriminative and straightforward detection between OP and non-OP neurotoxins was successfully achieved with cyclic voltammetry (CV) and UV–vis methods on the MWCNT–$(PEI/DNA)_2$/OPH/AChE biosensor, showing great potential in large screening of OP and non-OP pesticides in practical applications.

1. Introduction

Development of highly sensitive and discriminative techniques for detection of toxic analytes has been one of the top research priorities in the past few decades. Extensive use of pesticides and the release of tremendous amounts of their residues in the environment such as soil, water and food raised serious public concerns regarding health, environment and food safety (Gupta and Melatovic, 2012). Organophosphates (OP) and carbamates (non-OP) are highly neurotoxic compounds, and with much lower doses can cause chronic delayed onset toxicity to nerve cells. Several studies have shown that low-level exposure of these pesticides attribute to the inhibition of the acetylcholine esterase (AChE) enzyme, which regulates the turnover of the neurotransmitter acetylcholine in synaptic transmission. Consequently, acetylcholine accumulation in receptor sites can lead to various clinical complications, ultimately leading to death (Fukuto, 1990; Williams et al., 1997). Therefore, their detection in environmental and biological samples using sensitive and discriminative methods is highly demanded. Chromatography based traditional instrumentation—HPLC, GC–MS and LC–MS—are the most important OP and non-OP detection methods. However, these methods require meticulous and labor-intensive sample preparations, and sophisticated, expensive instruments.

Acetylcholine esterase (AChE) inhibition-based electrochemical biosensors have received high attention for analyzes of pesticide compounds, based on their simplicity, rapidity, high specificity, and reduced sample preparation (Kirsch et al., 2013; Kulys and D'Costa, 1991; Mionetto et al., 1994; Palleschi et al., 1992). The inhibition mechanism involves high affinity of both OPs and non-OPs toward the AChE enzyme where the hydroxyl of the serine residue within the active site is phosphorylated (OPs) or

* Corresponding author. Tel.: +1 334 844 4485.
E-mail address: als@auburn.edu (A.L. Simonian).
[1] Authors contributed equally in this work.

http://dx.doi.org/10.1016/j.bios.2014.08.036
0956-5663/

carbamylated (non-OPs). Several other enzymes including butrylcholine esterase (L. Wang et al., 2011), and urease (Sassolas et al., 2012; Starodub et al., 1999) have been used in the development of a variety of electrochemical biosensors based on inhibition mode in which the signal from electroactive products is inversely proportional to the pesticide concentration. Various other inhibition sensors have been developed on bi-enzyme cascade reactions AChE and Choline Oxidase (ChOx) for recognizing acetylcholine/choline based on amperometric detection of H_2O_2 (Hou et al., 2012; Meng et al., 2013; Zheng et al., 2011). Although the majority of present biosensors are inhibition/catalytic based, remarkably, all of them are based on "one analyte—one biorecognition element" detection pathway which is not specific enough to derive a conclusion, and thus rendering it impossible to discriminate a series of key pesticide analytes. In contrast, if measured with more than one biorecognition structure/element and is targeted the same analyte, an unambiguous result can be achieved. In this line, multi-enzyme biosensing systems that provide versatility for detection of multi-analytes open up new possibilities for multiplexed assays of different chemical analytes.

Recently, organophosphate hydrolase (OPH) was recognized as an alternative recognition enzyme for direct detection of organophosphate (Dave et al., 1993; Dumas et al., 1990). The enzyme hydrolyzes the OP molecule, the detection signal is directly proportional to the concentration of the OP and the products can be measured by spectrophotometric and electrochemical means. In 1996, we pioneered a new "kinetic" approach for the direct detection of OP neurotoxins based on the enzyme OPH. It has been demonstrated that the enzymes cleave the P–O, P–F, P–S or P–CN bonds, which can result in changes in pH, that can be directly detected by electrochemical (Rainina et al., 1996) and optical techniques (Russell et al., 1999; Simonian et al., 2005). Flow injection amperometric detection of OP nerve agents based on OPH biosensor was also reported (Wang et al., 2003). Simonian et al. (2001a, 2001b, 1997) further identified a novel multi-enzyme strategy for discrimination between different classes of neurotoxins.

Recent advances for development of enzyme-based biosensors have focused on incorporating enzymes with novel nanomaterials of fascinating electronic, mechanical and optical properties, e.g. carbon nanotubes (CNTs) (Feng and Ji, 2011), graphene oxide (Y. Wang et al., 2011; Zhang et al., 2010), nanoparticles (Upadhyay et al., 2009; Zhao et al., 2013), and quantum dots (Meng et al., 2013) etc. For example, CNT modification enhances direct electron transfer for electrochemical-based biosensors and provides excellent scaffolding structures for enzymes while retaining their bioactivities, resulting in an overall performance of biosensors with improved features such as a faster response time, signal amplification, higher sensitivity, better selectivity and stability. A key issue in these novel biosensors is the method of enzyme immobilization onto nanomaterials and their integration in biosensors. Ideally, a method that allows for high loading, retention of biological activity, nanomaterial properties, simplicity and control of the film architecture is desired. To overcome these challenges, a diverse set of CNT immobilization strategies for enzyme immobilization was developed and largely presented in the literature. Physical adsorptions were reported between enzymes and modified/functionalized nanomaterial surfaces through electrostatic interactions (Wang et al., 2003; Zhang et al., 2010). Although this method is relatively simple, requiring no cross-linking reagents, enzyme leaching is the major problem (Brady and Jordaan, 2009). Covalent immobilization facilitates strong amide bonding between enzyme and functionalized nanomaterials or covalent linkage of enzyme and nanomaterials via coupling reagents (Lin et al., 2004; Liu et al., 2010). Other methods including electropolymerization (Huang et al., 2013). Layer-by-layer (LbL) assembled multilayer interfaces were also reported. LbL assembly, due to its simplicity and versatility, has emerged as one of the most popular approaches for the fabrication of biofunctionalized multilayers, based on the alternating assembly of oppositely charged layers. It has been demonstrated to be an effective approach for the attachment of a variety of enzymes onto CNTs and self-assembly of organized CNT-biopolymer/CNT-enzyme multilayered biosensors (Batra and Pundir, 2013; Liu et al., 2010; Mantha et al., 2010; Nepal et al., 2008; Wooten et al., 2014). Previously, our group has reported on LbL assembly of CNTs coatings armored with lysozyme with precisely controlled thickness/alignment and LbL self-assembly processes for fabrication of MWCNT–OPH/MWCNT–DNA multilayer biosensor for organophosphate detection (Mantha et al., 2010).

Here, we report the fabrication of a novel nanotechnology-enabled multianalyte biosensor platform based on intercalation of CNTs covered with oppositely charged biopolymers and enzymes, for the assembly of unique multifunctional nanointerfaces for discriminative detection of OP and non-OP pesticides. To achieve this goal, LbL assembly of electrostatically interacted enzyme-armored MWCNT–OPH and MWCNT–AChE with a set of cushioning bilayers consisting of MWCNT–polyethyleneimine (PEI) and MWCNT–DNA on glassy carbon electrode was fabricated. The key idea is the combination of a direct catalytic OP hydrolyzes reaction and an inhibition-based AChE reaction renders a discriminative screening of OP and non-OPs from unknown samples. We report fabrication, optimization and characterization of LbL bio-nanostructure biosensor using surface plasmon resonance technique (SPR), electrochemical impedance spectroscopy (EIS), cyclic voltammetry (CV) and UV–vis spectrophotometry for discriminative detection between paraoxon (a model of OP) and carbaryl (a model of non-OPs) with high specificity and sensitivity.

2. Materials and methods

2.1. Materials

OPH was isolated from a recombinant *Escherichia coli* strain using published procedures (Dumas et al., 1990). Paraoxon (PX) was obtained from ChemService, Inc. (West Chester, PA) and dissolved in DI water and stirred at 4 °C for at least 72 h before use. Carbaryl (1-Naphthyl-N-methylcarbamate, 559814), multi-walled carbon nanotubes (MWCNTS) (95% purity, 1–5 μm length, 30 ± 10 nm diameter), acetylcholine esterase (AChE) from electrophorus electricus eel (E.C 3:1:1:7, 518 U/mg solids), lyophilized salmon sperm DNA salt, N-hydroxysulphosuccinimide (NHS), N-ethyl-N-(3-dimethylaminopropyl) carbodiimide hydrochloride (EDC), polyethyleneimine (PEI), Acetylcholine Chloride (ATCh) $\geq$ 99%, 4-Aldrithiol (98%), 2-(N-morpholino) ethanesulfonic acid (MES), N-cyclohexyl-2-aminoethanesulfonic acid (CHES), phosphate buffered saline (PBS), tris(hydroxymethyl)aminomethane (TRIS), potassium ferricyanide $K_3Fe(CN)_6$ and potassium ferricyanide $K_4Fe(CN)_6$ were all obtained from Sigma-Aldrich (St. Louis, MO). Dimethyl sulphoxide (DMSO) A.C.S. grade and Acetonitrile were obtained from Fischer Scientific. Ultrapure DI water obtained from Millipore Direct-Q Water system (resistivity, 18.2 MΩ cm^{-2}) was used for all the sample preparations.

2.2. Preparation of enzyme/polymer nanocomposites

The OPH and AChE were immobilized onto carboxylated MWCNTs by NHS/EDC carbodiimide chemistry via two-step process (Pedrosa et al., 2008). Briefly, 2 mg of carboxylated MWCNT was dispersed into 2 mL of MES buffer (50 mM, pH 4.7) followed by the addition of 1 mL of 20 mM NHS and 1 mL of 320 mM EDC.

Please cite this article as: Zhang, Y., et al., Biosensors and Bioelectronics (2014), http://dx.doi.org/10.1016/j.bios.2014.08.036

The solution was stirred for 30 min and filtered through 0.2 μm polycarbonate membrane under vacuum filtration with thorough rinsing with a MES buffer (50 mM, pH 6.2) to remove any excess unbound NHS and EDC. The as-prepared MWCNT–NHS ester conjugate was re-dispersed into 3 mL phosphate buffer (0.1 M, pH 8.3) and 400 U of AChE, or 562 U of OPH, was added into the solution for enzyme immobilization. The immobilization process was allowed to proceed overnight on a platform shaker at 4 °C. The MWCNT–AChE or MWCNT–OPH precipitate was then centrifuged (13,200 rpm, for 30 min) and subsequently rinsed with a MES buffer three times. After centrifugation purification, the MWCNT–AChE and MWCNT–OPH were suspended in 1 mL of TRIS buffer (20 mM, pH 7.5) and 1 mL CHES buffer (20 mM, pH 8.9), respectively, and stored in a refrigerator (4 °C) for further use.

Preparation of MWCNT–PEI and MWCNT–DNA was based on the previously reported protocol (Mantha et al., 2010). Two milligram carboxylated MWCNT was dispersed in 10 mL of 1 mg/mL PEI solution, followed by tip-sonication for 1 h in ice bath. After centrifugation purification, the prepared MWCNT–PEI sediment was re-dispersed into 5 mL of deionized water. MWCNT–DNA was prepared with a similarly described process. Stock solutions of 0.4 mg/mL MWCNT–PEI and MWCNT–DNA were obtained as final concentrations, which were stored at 4 °C until further use.

2.3. Electrode preparation and modification

Prior to casting the nanocomposites, the GCE electrode was activated through alumina polishing and subsequent amperometric treatment with 1 M NaOH at 1.2 V vs. Ag/AgCl for 5 min. The negatively charged electrode was rinsed and dried with high purity nitrogen gas. Then 20 μL of positively charged MWCNT–PEI nanocomposite suspension was drop cast onto the GCE and left drying at room temperature for 15 min to allow sufficient electrostatic interaction. The modified electrode was rinsed with DI water to remove the unbound MWCNT–PEI and dried. Subsequently, 20 μL of negatively charged MWCNT–DNA was deposited, followed by 15 min drying–rinsing and drying. This was followed by deposition of another bilayer of MWCNT–$(PEI/DNA)_2$ to serve as strong cushion layers for further assembly (Fig. 1). Twenty microliters of MWCNT–OPH/MWCNT–AChE was deposited upon the cushion layers, dried-rinsed with PBS buffer. The prepared nanostructured biosensor was stored in 4 °C before use.

2.4. LbL interface optimization and evaluation of biosensor

To achieve the optimal biosensor configuration, an analysis of substrate penetration through the layers was conducted. Assembly of the AChE nanocomposite within varying inter-layers (bottom to top position: 2nd 4th, 6th, 8th) on the 8 layered structure, the total number of nanostructured layers (2, 4, 6, 8, 10) and different amounts of CNTs were used to optimize the LbL formation by measuring the corresponding amperometric response towards acetylthiocholine (ATCh) at a fixed concentration of 125 μM. Configuration of the resulting multilayered bi-enzyme biosensor (Fig. 1) was utilized for further characterization.

2.5. SPR monitoring of LbL self-assembly

SPR experiments were performed with SPREETA™ Texas Instruments (Dallas, TX, USA) using the Multi-SPR software package. The SPR technique was used for the real-time monitoring of the self-assembly process of MWCNT–$(PEI/DNA)_2$/OPH/AChE on a gold surface. Prior to installation, the SPR gold sensor surface was meticulously cleaned with a piranha solution (H_2SO_4 and H_2O_2 (3:1)) for 3 min and thoroughly rinsed with deionized water, followed by 2 min of plasma cleaning. (*Attention: caution must be taken as the piranha solution readily causes chemical burns and is highly reactive, particularly with organic materials.*) The experimental set-up was then initialized in the air and calibrated with DI water (refractive index (RI): 1.3333). DI water was pumped into the flow cell on to the SPR gold sensor surface through two inlet channels until the baseline reached a stable value. The LbL self-assembly was initiated by flowing positively charged MWCNT–PEI into the flow cell at a constant flow rate (50 μL/min) over the negatively charged surface of the gold chip. This was followed by subsequent pumping of negatively charged MWCNT–DNA and two bilayers of MWCNT–PEI/DNA as a cushion support. Upon achieving stable value, MWCNT–OPH/AChE was flowed across to form LbL MWCNT–$(PEI/DNA)_2$/OPH/AChE on the gold surface. Before injection of the enzyme layers, 20 mM CHES buffer and 20 mM TRIS buffer were injected as a background signal.

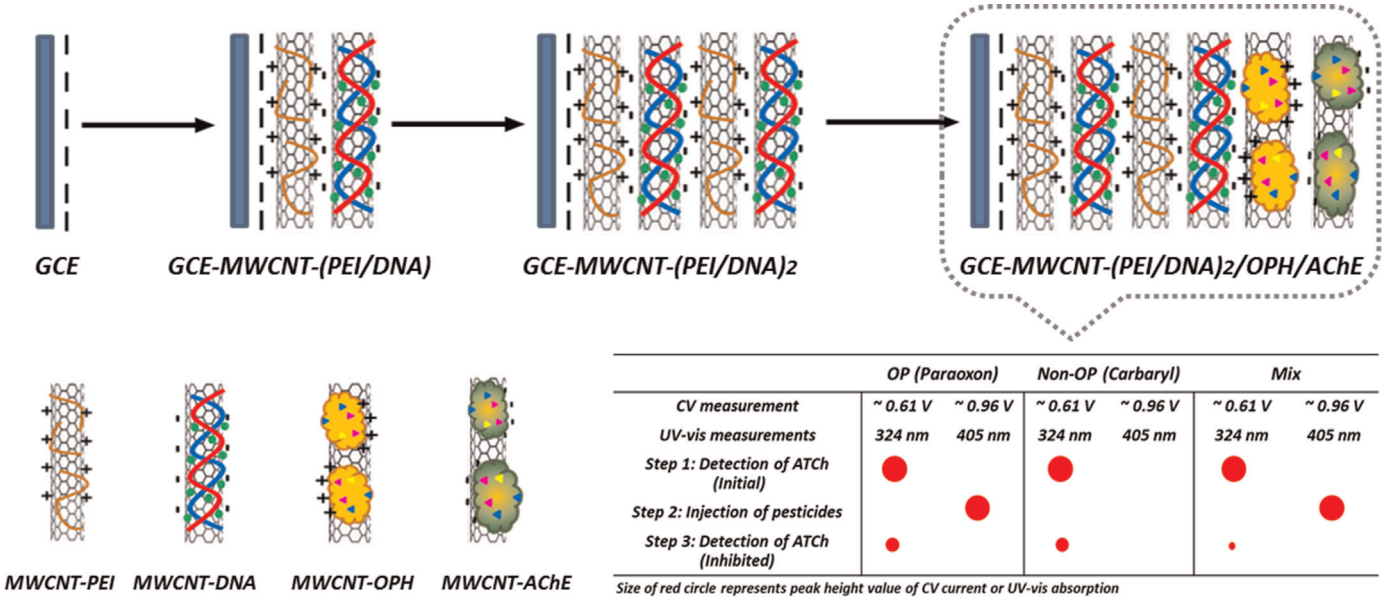

Fig. 1. Schematic illustration of LbL assembly and bi-enzymatic layer in biosensor interfaces constructed on the GCE and discriminative detection of OP and non-OP using electrochemical and optical methods.

Please cite this article as: Zhang, Y., et al., Biosensors and Bioelectronics (2014), http://dx.doi.org/10.1016/j.bios.2014.08.036

2.6. Electrochemical and UV–vis measurements

Cyclic voltammetric experiments were performed using an electrochemical analyzer CHI 660 (CH Instruments, Austin, TX) potentiostat connected to a computer with a chi990b software package. The electrochemical impedance spectroscopy (EIS) data was collected with Gamry Instruments Reference 600 potentiostat/galvanostat/ZRA connected to a computer with Gamry Echem Analyst software. A conventional three-electrode system consisting of bare or modified glassy carbon electrode (GCE, 3-mm diameter) as a working electrode, Ag/AgCl (3 M KCl) as the reference and platinum wire as a counter electrode was used. EIS was performed in 0.4 M KCl solution at the formal potential (0.22 V) of $[Fe(CN)_6]^{3-/4-}$ with a frequency range from 100 kHz to 0.01 Hz, amplitude of 5 mV in 1 mM $K_3Fe(CN)_6/K_4Fe(CN)_6$ solution (1:1) mixture as electroactive probe. Cyclic voltammograms of $[Fe(CN)_6]^{3-/4-}$ were carried out in a 0.4 mM KCl solution containing 1 mM $K_3Fe(CN)_6/K_4Fe(CN)_6$ (1:1) mixture at scan rate of 0.1 V/s. Pesticide detection by cyclic voltammogram and UV–vis experiments were conducted using a 10 mM PBS buffer, pH 7.4. UV–vis spectrophotometer (Amersham Biosciences Ultrospec 2100 pro) with 1 mL PMMA cuvettes was used for collecting UV–vis absorption spectrum data. All experiments were carried out at room temperature (25 ± 2 °C).

2.7. Inhibition of AChE with OP and non-OP

The MWCNT–$(PEI/DNA)_2$/OPH/AChE biosensor was employed for discriminative detection of OP and non-OP using a three step process. First, the electrode was tested for initial CV responses in a 10 mM PBS buffer pH 7.4 containing 1 mM ATCh (5 min reaction with stirring before test). In the second step, inhibition assays were performed by incubating the electrode in the desired concentrations of pesticides for 15 min. Finally, the electrode was rinsed and tested again in a fresh solution of 1 mM ATCh in similar conditions. The inhibition percentage of AChE was calculated using Eq. (1)

$$\frac{I_0 - I_{inhibition}}{I_0} \times 100\% \quad (1)$$

where I_0 and $I_{inhibition}$ are the signals obtained in steps 1 and 3. Inhibition (%) vs. concentration of OP and non-OP were plotted to obtain linear calibration graphs.

2.8. Real sample detection

Apples were bought from a local supermarket in Auburn, Alabama. Prior to the sample preparation, the apples were washed and cleaned with 5% acetonitrile (Valdés-Ramírez et al., 2008) to eliminate potential pesticide contamination. 10 mM PBS buffer

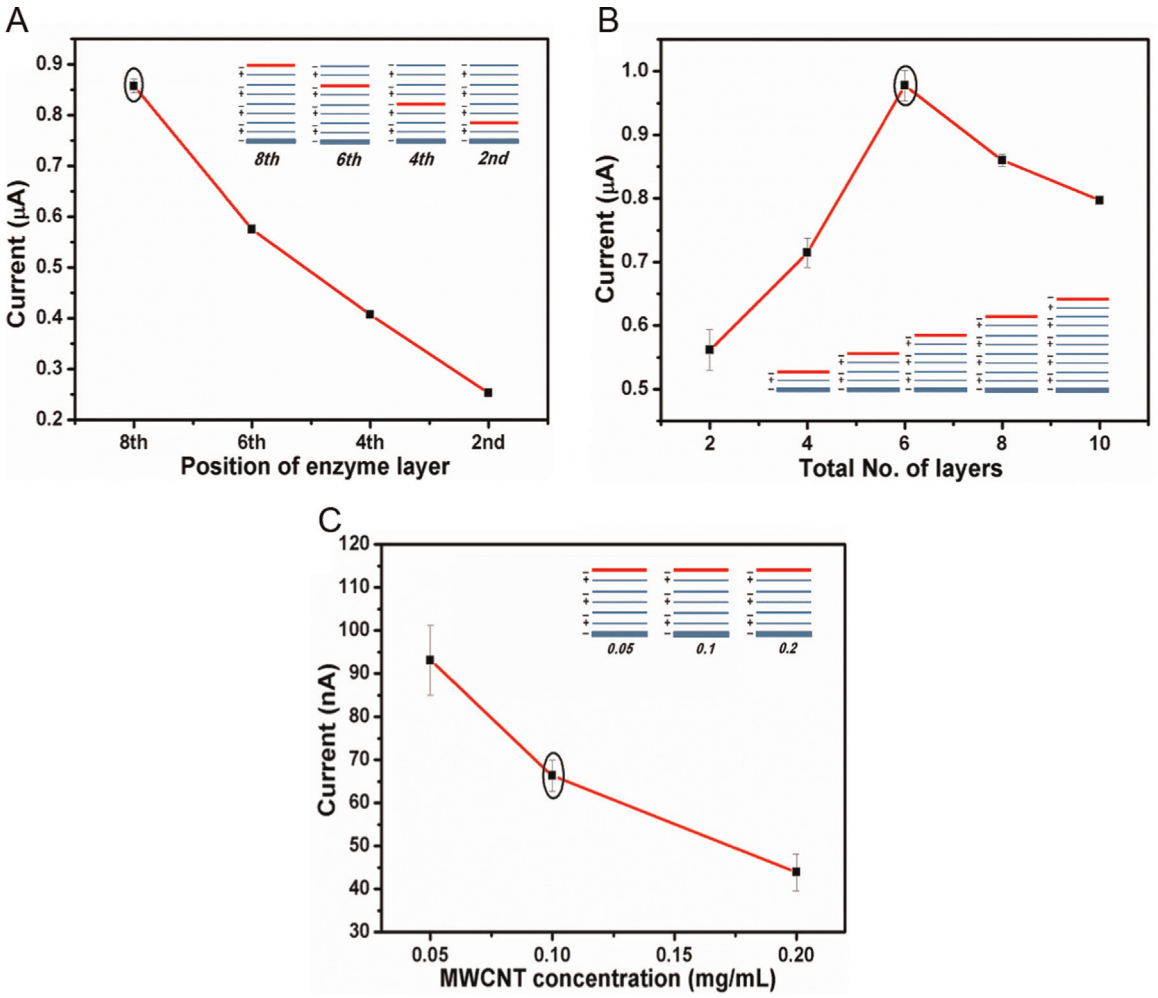

Fig. 2. LbL assembly of enzyme nanostructure with various parameter optimizations: (A) position of enzyme layer, (B) total number of layers with enzyme on the top, and (C) MWCNT concentration. The final optimized parameters were achieved when AChE layer was at terminal position (A) with total number of 6 layers (B) using 0.1 mg/mL cushion CNT–$(PEI/DNA)_2$ layers (C).

Please cite this article as: Zhang, Y., et al., Biosensors and Bioelectronics (2014), http://dx.doi.org/10.1016/j.bios.2014.08.036

was first spiked with a known concentration of paraoxon or carbaryl and sprayed onto the apple skin that was peeled and cut into 2 cm × 2 cm pieces. The samples were allowed to stand for 15 min, dissolved with 1 mL 5% acetonitrile, and vortexed to extract the pesticide. The solvent was dried in fume hood, and then the residues were reconstituted with 200 μL of PBS buffer followed by inhibition analyzes with MWCNT–$(PEI/DNA)_2$/OPH/AChE bi-enzymatic biosensor. Paraoxon and carbaryl quantities were calculated using standard curves that were obtained from known concentrations of pesticides.

3. Results and discussion

3.1. Optimization of LbL nano-structured biosensor

As shown in Fig. 2A, the sequence of the position of MWCNT–AChE layer within the biopolymer interlayers attributed to the permeability of substrate reaching the enzyme. As more layers covered onto MWCNT–AChE, the amperometric response decreased due to less permeability of the substrate to the enzyme. Therefore, the highest enzyme activity was achieved when a MWCNT–AChE layer was placed at the terminal 8^{th} layer. The functionality and optimization of cushioning layers is shown in Fig. 2B. By increasing the MWCNT–PEI/DNA layers, we could easily control the thickness of the cushioning layers and thus the peak current of the resulting electrodes with enzyme immobilized on the top layer. Increasing the number of cushion layers in analyzing total number of layers from 2 to 10, increased the current signal from 2 to 6 layers. However, then dropped from 8 to 10 layers. Therefore, the optimized total number of layers where maximum current was achieved was found to be 6 layers. This was further used for conducting pesticide detection measurements. As such the cushion layers of polyelectrolyte CNTs play an important role in enhancing the efficiency of electron transfer. We believe that the lower number of layers had an easy diffusion of the substrate molecules and good electron transfer to the electrode surface while increased number of layers led to a thicker surface and a high resistance (Hou et al., 2012). The optimized concentrations of MWCNTs obtained were 0.1 mg/mL for MWCNT–PEI and MWCNT–DNA and 0.2 mg/mL for MWCNT–AChE and MWCNT–OPH (Fig. 2C).

3.2. SPR characterization of LbL self-assembly

Fig. 3A demonstrates the stepwise formation of LbL self-assembly between MWCNT–PEI ($\Delta RU = 97.38 \pm 2.57$, $\Delta RI = 0.9834 \times 10^{-4}$) and MWCNT–DNA ($\Delta RU = 1444.05 \pm 64.83$, $\Delta RI = 1.4246 \times 10^{-3}$) with additional bilayers of MWCNT–PEI ($\Delta RU = 455.72 \pm 52.03$, $\Delta RI = 4.7611 \times 10^{-4}$) and MWCNT–DNA ($\Delta RU = 1865.39 \pm 55.16$, $\Delta RI = 1.8429 \times 10^{-3}$). ΔRU (1RU = 10^{-6} RI unit) values represent the change in response units (RU) between the initial signal and stabilized signal for each layer. The strong electrostatic interactions between bilayers of PEI and DNA served as cushion support for immobilization of cationic OPH and anionic AChE layer. The CHES and TRIS buffers set apart the enzyme

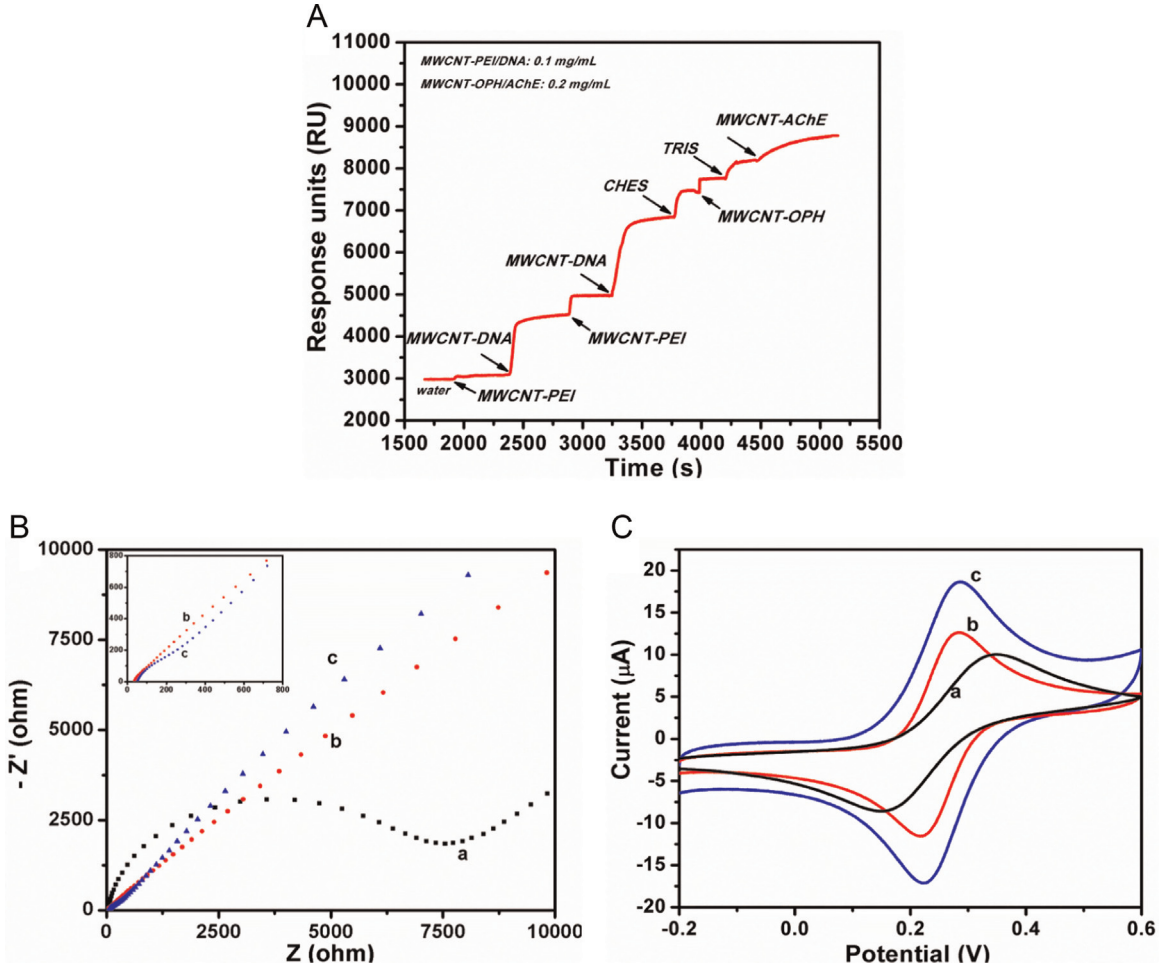

Fig. 3. (A) SPR real time monitoring of LbL self-assembly process for desired LbL nanostructure. (B) EIS and (C) CV of (a) bare GCE, (b) GCE–MWCNT–$(PEI/DNA)_2$, (c) GCE–MWCNT–$(PEI/DNA)_2$/OPH/AChE; bare and modified electrodes in 0.4 M KCl containing 1 mM $[Fe(CN)_6]^{3-/4-}$ (1:1) with a frequency range from 100 kHz to 0.01 Hz with an amplitude of 5 mV.

Please cite this article as: Zhang, Y., et al., Biosensors and Bioelectronics (2014), http://dx.doi.org/10.1016/j.bios.2014.08.036

nanocomposites from their isoelectric points to exhibit sufficient charges required for LbL formation. Injection of buffers slightly increased the RU signal which were further subtracted as background for MWCNT–OPH ($\Delta RU = 277.14 \pm 10.91$, $\Delta RI = 2.8574 \times 10^{-4}$) and MWCNT–AChE ($\Delta RU = 573.14 \pm 28.94$, $\Delta RI = 5.9278 \times 10^{-4}$) binding. SPR study was successfully employed for visualization of formation of six-layered MWCNT–$(PEI/DNA)_2$/OPH/AChE biosensing interfaces on gold surface, indicating the effectiveness of electrostatically interacted LbL self-assembly processes.

3.3. Electrochemical characterization of modified electrode

The bare and surface modified electrode were investigated using EIS and CV with $[Fe(CN)_6]^{3-/4-}$ as redox probe. Fig. 3B and

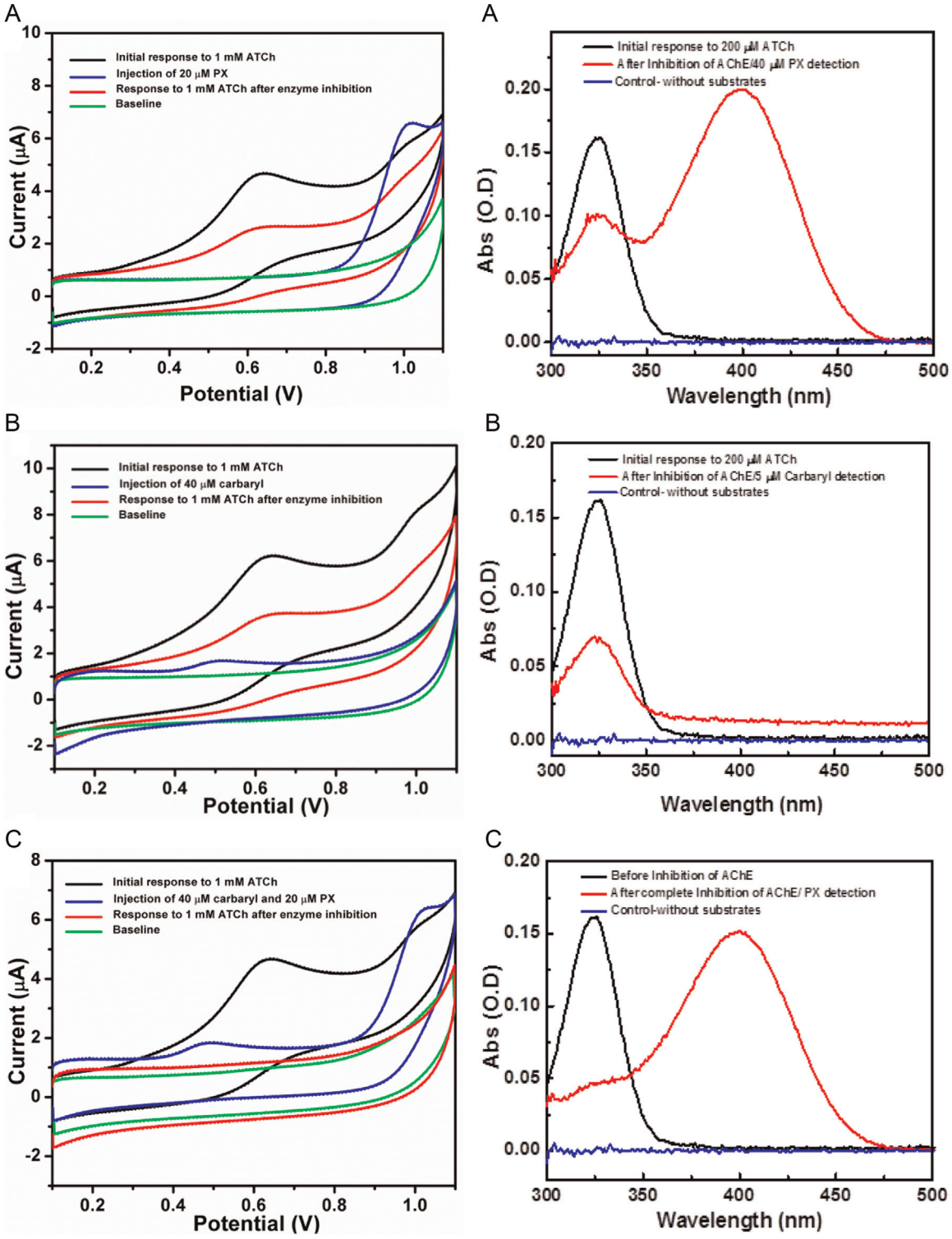

Fig. 4. Left: CV response for discriminative detection of (A) OP (20 μM paraoxon), (B) non-OP (40 μM carbaryl) and (C) mix of OP (20 μM paraoxon)and non-OP (40 μM carbaryl). Right: Optical absorbance measurements for discriminative detection of (A) OP (40 μM paraoxon), (B) non-OP (5 μM carbaryl) and (C) mix of OP (40 μM paraoxon) and non-OP (5 μM carbaryl). (For interpretation of the references to color in this figure, the reader is referred to the web version of this article.).

Please cite this article as: Zhang, Y., et al., Biosensors and Bioelectronics (2014), http://dx.doi.org/10.1016/j.bios.2014.08.036

C illustrates the results of impedance spectroscopy on (a) GCE, (b) MWCNT–(PEI/DNA)$_2$ and (c) MWCNT–(PEI/DNA)$_2$/OPH/AChE. The Z' and $-Z''$ are the real and imaginary variables of impedance, respectively. Typically, the diameter of semicircle observed at higher frequencies of impedance (Nyquist) plot correspond to the charge transfer resistence (Rct) and the linear portion at lower frequency depicts diffusion limited process (Hou et al., 2012). It can be observed from Fig. 3B, the bare GCE shows Rct value of 8239 Ω (curve a) corresponding to huge charge transfer resistance. With addition of (MWCNT–PEI/MWCNT–DNA)$_2$ on the bare electrode, the Rct value dramatically decreased demonstrating excellent electron transfer between $[Fe(CN)_6]^{3-/4-}$ and electrode surface modified with functionalized-MWCNT layers. It can be observed that EIS (curve b) is almost a straight line suggesting that the electrode is diffusionally controlled. However, Rct slightly increased for MWCNT–(PEI/DNA)$_2$/OPH/AChE immobilized GCE (curve c), compared to MWCNT–(PEI/DNA)$_2$. The impedance results thus obtained by the change in electron transfer provide evidence for the successful LbL assembly of layers on GCE. The cyclic voltammograms corresponding to EIS experiments further supported the modification process as shown in Fig. 3C. The peak current (i_p) of the redox probe increased and the peak potential separation (ΔEp) decreased in the order of (a) GCE, (b) MWCNT–(PEI/DNA)$_2$ and (c) MWCNT–(PEI/DNA)$_2$/OPH/AChE. In addition to impedance measurements, effective surface area of three electrodes was obtained according to Randles Sevick equation (Ding et al., 2005)

$$I_{pa} = (2.69 \times 10^5) n^{3/2} A D^{1/2} \nu^{1/2} C \quad (2)$$

where n is the number of electrons transferred, I_{pa} is anodic peak current (A cm^{-2}), C is the concentration of $K_3Fe(CN)_6$ (mol cm^{-3}), D is the diffusion coefficient (cm^2 s^{-1}), ν is the scan rate (V/s) and A is the surface area of the electrode (cm^2). The value of D is considered as 0.65×10^{-5} cm^2 s^{-1} at 20 °C. CV were conducted in 1 mM $K_3Fe(CN)_6$/1 M KCl solution in a potential range of −0.2 to +0.65 V at varying scan rates (Supplementary material Fig. S1). By performing linear regression for I_{pa} vs. $\nu^{1/2}$ the slope can be obtained (Fig. S1), which was further used in Eq. (2). for calculating surface area of the electrode. The results indicate that the process is controlled by diffusion. The active surface area for bare GCE, MWCNT–(PEI/DNA)$_2$ and MWCNT–(PEI/DNA)$_2$/OPH/AChE was 0.0596 cm^2, 0.0787 cm^2 and 0.1078 cm^2 respectively. The surface area for bare GCE is in close agreement with the values previously reported (Ma et al., 2010). The six layered enzyme/polymer nanocomposite was found to have highest surface area.

3.4. Discriminative detection of OP and non-OP pesticides

3.4.1. Electrochemical approach

Discriminative detection of OP and non-OP pesticides was achieved with GCE–MWCNT–(PEI/DNA)$_2$/OPH/AChE bi-enzymatic biosensor using electrochemical approach. As shown in Fig. 4A (right), cyclic voltammetry responses were examined on modified GCE before and after OP and non-OP inhibition. There was no anodic peak current (green curve) observed with modified GCE when no substrates were added to pH 7.4, 10 mM PBS buffer. However, CV responses showed a peak current (black curve) at 0.61 V vs. Ag/AgCl, when 1 mM ATCh was added. This peak was attributed to the oxidation of thiocholine (Pandey et al., 2000), hydrolysis product of ATCh which was considered as the initial response of the biosensor. Detection of OP using 20 μM paraoxon was measured based on AChE partial inhibition at detection potential of 0.61 V vs. Ag/AgCl (oxidation of thiocholine). It can be observed from red curve that the peak current decreased and 58.02 ± 3.4% was obtained. This result was further confirmed by direct catalytic hydrolysis of OPH producing p-nitrophenol which undergoes oxidation showing significant peak current (blue curve) at detection potential 0.96 V vs. Ag/AgCl. For non-OP detection, carbaryl (40 μM) is not hydrolyzed by OPH showing no peak current at potential 0.96 V and therefore, it can only be determined based on AChE inhibition percentage (56.93 ± 4.1%) by measuring thiocholine at 0.61 V as shown in Fig. 4B (right). In combination of both OP (20 μM paraoxon) and non-OP (40 μM carbaryl), discriminative detection was achieved by complete inhibition (94.03 ± 2.7%) of AChE enzyme showing no peak current at 0.61 V while significant peak current for p-nitrophenol at 0.96 V was observed from Fig. 4C (right).

3.4.2. UV–vis approach

The UV–vis measurements of discriminative detection was performed directly on modified screen printed electrode with the same method as fabrication of GCE–MWCNT–(PEI/DNA)$_2$/OPH/AChE. The electrode was initially tested by UV–vis measurements in pH 7.4, 10 mM PBS buffer containing 200 μM ATCh at a wavelength ranging from 300 nm to 600 nm by measuring thiocholine oxidation reaction with 0.1 mM 4-Aldrithiol (stock solution of 12 mM 4-Aldrithiol was prepared in DMSO) producing 4-thiopyridine (WRAIR Assay) which gives observable peak at λ324 nm (Haigh et al., 2008). Fig. 4A (left) black curve displays the optical absorbance at λ324 nm (absolute peak Abs = 0.16 ± 0.0041 O.D.). Detection of OP (40 μM paraoxon) was based on AChE partial non-competitive inhibition using WRAIR assay. The inhibition level is separated from the initial by ΔAbs = 0.09 ± 0.0058 O.D. This can be further confirmed by measuring 40 μM paraoxon by OPH hydrolysis producing para-nitrophenol which displays peak (absolute Abs = 0.19 ± 0.016 O.D.) at λ405 nm as shown as red curve in Fig. 4A (left). However, in case of non-OP (5 μM carbaryl) which has no absorption band peak can only be detected based on AChE partial non-competitive inhibition, at λ324 nm (ΔAbs = 0.069 ± 0.0054 O.D.) as shown in Fig. 4B (left). Discriminative detection of OP (paraoxon) and non-OP (Carbaryl) in combination was achieved based on AChE total non-competitive inhibition at λ324 nm (ΔAbs = 0.12 ± 0.0062 O.D.) with decreased absorbance signal while detecting p-nitrophenol at λ405 nm (absolute Abs = 0.15 ± 0.011 O.D.). All absorbance spectra data were collected after 5 min of enzymatic reactions before (without pesticide) and after inhibition (with 3 min pesticide incubation) (Fig. 4C (left)). Control experiments were conducted without substrates added to the buffer electrolyte solution.

3.4.3. Analytical performance

Sensitivity, linearity and dynamic range were investigated for MWCNT–(PEI/DNA)$_2$/OPH/AChE bi-enzymatic biosensor. Paraoxon was determined by both OPH (catalytic) and AChE inhibition based assays, while carbaryl was determined solely by the inhibition method. Based on inhibition percentage as shown in Fig. 5A and B, the linear response range for paraoxon and carbaryl was 0.5–40 μM and 10–80 μM with dynamic range 0.5–50 μM and 10–100 μM respectively. The linear regression equation, $y = 0.021x + 0.09135$ with a correlation coefficient (R^2) of 0.970 and $y = 0.00941x + 0.11178$ with R^2 of 0.9836 can be established for paraoxon and carbaryl, respectively. The limit of detection (LOD) obtained for paraoxon and carbaryl detection was 0.5 and 10 μM, respectively. Calibration measurements were conducted in triplicates and good reproducibility was achieved. Similarly, the linear range for direct detection of paraoxon (Fig. 5C) obtained was 1–64 μM with limit of detection (LOD) of 1 μM. The linear regression equation, $y = 0.07303x + 0.1113$ can be established with a correlation coefficient of 0.9842. In order to determine substrate concentration dependence, the biosensor was further analyzed by varying concentrations of ATCh (40–640 μM) without pesticide

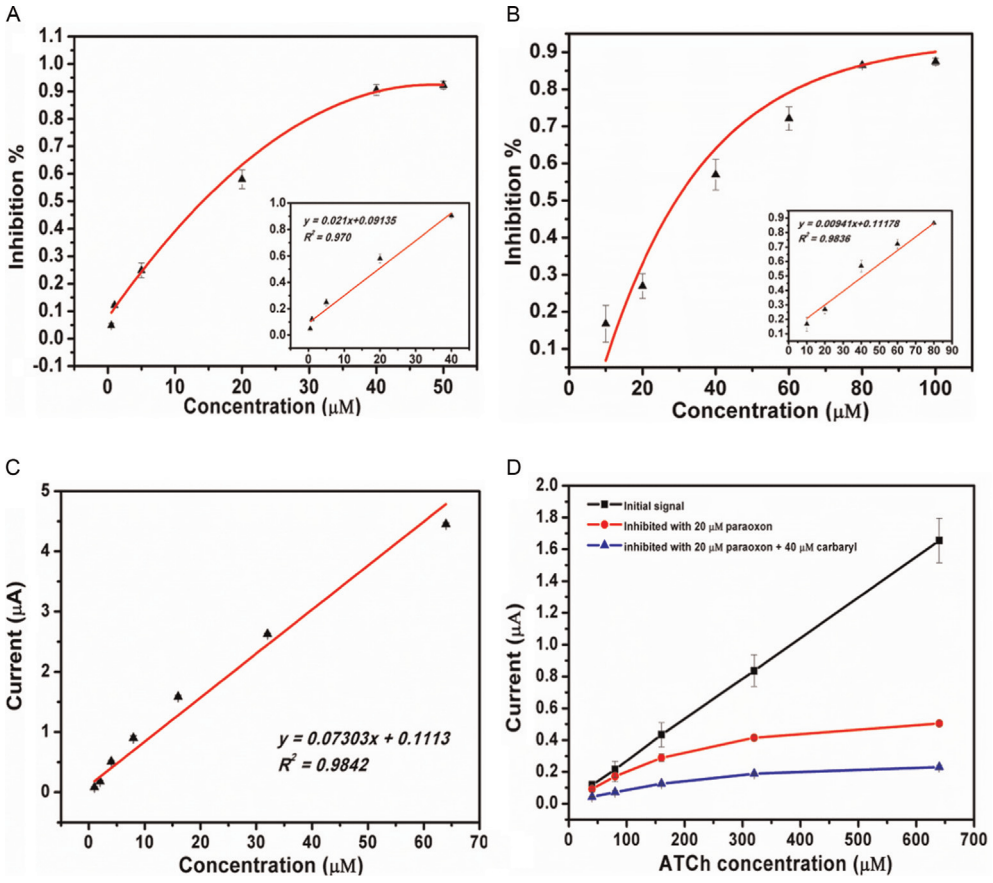

Fig. 5. Calibration curve for (A) paraoxon and (B) carbaryl on the bi-enzymatic biosensor through inhibition assay; (C) paraoxon through direct detection assay; (D) calibration curve for ATCh on (a) initial bi-enzymatic biosensor, (b) 20 μM paraoxon inhibited bi-enzymatic biosensor and (c) mix of 20 μM paraoxon and 40 μM carbaryl inhibited bi-enzymatic biosensor.

(initial), with 20 μM paraoxon and both 20 μM paraoxon and 40 μM carbaryl. The anodic peak current at 0.61 V vs. Ag/AgCl was measured. It can be clearly observed from Fig. 5D, due to high catalytic activity of the enzyme the peak current increased with increasing concentration of ATCh showing linear dependence. However with inhibitors there is decrease in peak current already at 100 μM ATCh and tend to be saturated with higher concentrations. For real samples, the inhibition percentage calculated from the blank sample was found to be 37.06% for paraoxon and 61.2% for carbaryl. The concentrations were further determined to be about 13.3 μM and 53 μM, respectively.

With this study, the MWCNT–$(PEI/DNA)_2$/OPH/AChE bi-enzymatic biosensor showed an good sensitivity and good linearity in nM–μM range of detection for paraoxon and carbaryl, demonstrating the proof of concept of the proposed bi-enzymatic biosensor for analyzes of OP, non-OP and both.

4. Conclusions

In this study, LbL self-assembly was successfully employed in development of MWCNT–$(PEI/DNA)_2$/OPH/AChE bi-enzymatic biosensor in discriminating between paraoxon and carbaryl pesticides by electrochemical and optical methods. The results demonstrated for the first time the potential for applying bi-enzymatic biosensing system in screening and discriminating two major class of pesticides, OP and non-OP. The cyclic voltammetric results provided good sensitivity, stability and reproducibility. In addition, the biosensor was able to detect pesticides extracted from real samples. In future, we anticipate that this versatile LbL self-assembly approach can be extended to a variety of enzyme to develop multi-enzyme biosensing strategy showing great advantages in multi-analyte discriminative monitoring on single platform for novel biosensing applications.

Acknowledgements

Financial supports in this study were from National Science Foundation grants (CBET-1317635), and the Auburn University Intramural Grants Program (AU-IGP). The author would also like to thank Sanjun Fan from Chemistry department for the help with impedance analyzes.

Appendix A. Supplementary information

Supplementary data associated with this article can be found in the online version at http://dx.doi.org/10.1016/j.bios.2014.08.036.

References

Batra, B., Pundir, C.S., 2013. Biosens. Bioelectron. 47, 496–501.
Brady, D., Jordaan, J., 2009. Biotechnol. Lett. 31, 1639–1650.
Dave, K.I., Miller, C.E., Wild, J.R., 1993. Chem. Biol. Interact. 87, 55–68.
Ding, S.J., Chang, B.W., Wu, C.C., Lai, M.F., Chang, H.C., 2005. Anal. Chim. Acta 554, 43–51.
Dumas, D.P., Durst, H.D., Landis, W.G., Raushel, F.M., Wild, J.R., 1990. Arch. Biochem. Biophys. 277, 155–159.
Feng, W., Ji, P., 2011. Biotechnol. Adv. 29, 889–895.
Fukuto, T.R., 1990. Environ. Health Perspect. 87, 245–254.

Gupta, R.C., Melatovic, D., 2012. In: Marrs, T.C. (Ed.), Mammalian Toxicology of Insecticides. Royal Society of Chemistry, Cambridge, UK, pp. 104–136.
Haigh, J.R., Lefkowitz, L.J., Capacio, B.R., Doctor, B.P., Gordon, R.K., 2008. Chem. Biol. Interact. 175, 417–420.
Hou, S., Ou, Z., Chen, Q., Wu, B., 2012. Biosens. Bioelectron. 33, 44–49.
Huang, Y., Wang, W., Li, Z., Qin, X., Bu, L., Tang, Z., Fu, Y., Ma, M., Xie, Q., Yao, S., Hu, J., 2013. Biosens. Bioelectron. 44, 41–47.
Kirsch, J., Siltanen, C., Zhou, Q., Revzin, A., Simonian, A., 2013. Chem. Soc. Rev. 42, 8733–8768.
Kulys, J., D'Costa, E.J., 1991. Biosens. Bioelectron. 6, 109–115.
Lin, Y., Lu, F., Tu, Y., Ren, Z., 2004. Nano Lett. 4, 191–195.
Liu, Y., Yu, D., Zeng, C., Miao, Z., Dai, L., 2010. Langmuir 26, 6158–6160.
Ma, Q., Ai, S., Yin, H., Chen, Q., Tang, T., 2010. Electrochim. Acta 55, 6687–6694.
Mantha, S., Pedrosa, V.A., Olsen, E.V., Davis, V.A., Simonian, A.L., 2010. Langmuir 26, 19114–19119.
Meng, X., Wei, J., Ren, X., Ren, J., Tang, F., 2013. Biosens. Bioelectron. 47, 402–407.
Mionetto, N., Marty, J.L., Karube, I., 1994. Biosens. Bioelectron. 9, 463–470.
Nepal, D., Balasubramanian, S., Simonian, A.L., Davis, V.A., 2008. Nanoscale 8, 1896–1901.
Palleschi, G., Bernabei, M., Tor, R., 1992. Sens. Actuators B 7, 513–517.
Pandey, P.C., Upadhyay, S., Pathak, H.C., Pandey, C.M.D., Tiwari, I., 2000. Sens. Actuators B Chem. 62, 109–116.
Pedrosa, V.A., Caetano, J., Machado, S.A.S., Bertotti, M., 2008. Sensors 8, 4600–4610.
Rainina, E.I., Simonian, A.L., Efremenco, E.N., Varfolomeyev, S.D., Wild, J., 1996. Biosens. Bioelectron. 11, 991–1000.
Russell, R.J., Pishko, M.V., Simonian, A.L., Wild, J.R., 1999. Anal. Chem. 71, 4909–4912.
Sassolas, A., Blum, L.J., Leca-Bouvier, B.D., 2012. Biotechnol. Adv. 30, 489–511.
Simonian, A., Efremenko, E., Wild, J., 2001a. Anal. Chim. Acta 444, 179–186.
Simonian, A., Grimsley, J., Flounders, A., Schoeniger, J., Cheng, T.C., DeFrank, J., Wild, J., 2001b. Anal. Chim. Acta 442, 15–23.
Simonian, A.L., Good, T.A., Wang, S.S., Wild, J.R., 2005. Anal. Chim. Acta 534, 69–77.
Simonian, A.L., Rainina, E.I., Wild, J.R., 1997. Anal. Lett. 30, 2453–2468.
Starodub, N.F., Kanjuk, N.I., Kukla, A.L., Shirshov, Y.M., 1999. Anal. Chim. Acta 385, 461–466.
Upadhyay, S., Rao, G.R., Sharma, M.K., Bhattacharya, B.K., Rao, V.K., Vijayaraghavan, R., 2009. Biosens. Bioelectron. 25, 832–838.
Valdés-Ramírez, G., Fournier, D., Ramírez-Silva, M.T., Marty, J.L., 2008. Talanta 74, 741–746.
Wang, J., Krause, R., Block, K., Musameh, M., Mulchandani, A., Schöning, M.J., 2003. Biosens. Bioelectron. 18, 255–260.
Wang, L., Du, D., Lu, D., Lin, C.T., Smith, J.N., Timchalk, C., Liu, F., Wang, J., Lin, Y., 2011. Anal. Chim. Acta 693, 1–6.
Wang, Y., Zhang, S., Du, D., Shao, Y., Li, Z., Wang, J., Engelhard, M.H., Li, J., Lin, Y., 2011. J. Mater. Chem. 21, 5319–5325.
Williams, F.M., Charlton, C., De Blaquière, G.E., Mutch, E., Kelly, S.S., Blain, P.G., 1997. Hum. Exp. Toxicol. 16, 67–71.
Wooten, M., Karra, S., Zhang, M., Gorski, W., 2014. Anal. Chem. 86, 752–757.
Zhang, J., Zhang, F., Yang, H., Huang, X., Liu, H., Zhang, J., Guo, S., 2010. Langmuir 26, 6083–6085.
Zhao, Y., Zhang, W., Lin, Y., Du, D., 2013. Nanoscale 5, 1121–1126.
Zheng, Z., Li, X., Dai, Z., Liu, S., Tang, Z., 2011. J. Mater. Chem. 21, 16955–16962.

Please cite this article as: Zhang, Y., et al., Biosensors and Bioelectronics (2014), http://dx.doi.org/10.1016/j.bios.2014.08.036